Effect of ash on coal direct chemical looping combustion

Rahul Wadhwani*, Bikash Mohanty

Heat Transfer Research Lab, Department of Chemical Engineering,

Indian Institute of Technology, Roorkee

Roorkee, Uttarakhand, India – 247667

Email: rahul123wadhwani@gmail.com

Email: bmohanty@iitr.ernet.in

* Corresponding Author

Biographical Note:

Dr. Bikash Mohanty is associated with Department of Chemical Engineering, Indian Institute of Technology, Roorkee, India as a Professor. He is actively associated in teaching, research and consulting. He has worked in the fields of multiphase heat transfer, Process simulation and design, Process Integration and optimization and Fire Engineering. He is also the coordinator of Education Technology cell which develops NPTEL online courses.

Rahul Wadhwani did his Integrated Dual Degree from Department of Chemical Engineering, Indian Institute of Technology, Roorkee, India in the year 2014. He works in the field of CFD simulation, Processes Optimization, etc. At present he is doing his Ph.D. from Centre for Fire Safety and Risk Engineering, Victoria University, Melbourne, Australia on CFD modeling of bushfire.

Abstract:

Low ash content coal as a fuel for chemical looping combustion for the production of clean energy along with CO_2 capture has been well established. However, major coal deposits in the region of Asia-Pacific and Australia are of high ash content and thus, pose difficulties in utilization of this technology. Therefore, an attempt has been made in the present work to study chemical looping combustion of high ash coal. For this purpose a CFD model which incorporates both fuel and air reactors and their inter-connecting parts to simulate a real chemical looping pilot plant has been developed. The results obtained for sub-bituminous coal as well as metallurgical coke for the above reactor have been validated against the published data within an

error band of ± 7%-14%. The validated model is then used for two high ash content coals designated as A and B.

Simulated results show that for A and B, fuel conversions are 93.8% and 87.79% respectively and that purity of CO_2 in air reactor exhaust are 89.12% and 90.73%. It has also been observed that, components of ash such as CaO, Fe_2O_3 show significant reactivity at the operating conditions, whereas, SiO_2 exhibits almost negligible reactivity. Further, in case of high ash coal, due to its low carbon content, the fuel requirement increases to sustain operating conditions.

Keywords: High ash content coal, Chemical looping combustion, CFD simulation

Introduction:

The rising trend of energy usage and amount of CO_2 in atmosphere exceeding 400ppm mark has created an alarming situation and thus provides required impetus for the development of clean energy processes. Power generation through renewable energy sources like Solar, Wind and Geothermal appears to be promising; however, it is still a distant dream that these resources can meet the present energy demand. Further, nuclear energy, due to its constraints related to safety and spent fuel management, also creates impediment in its development and full use. The challenges offered by above energy resources are shifting the pressure towards the use of fossil fuel to meet the recent energy demands though, its depleting quality is a matter of concern and offering increased challenges in terms of its pre- and post- treatment. [1]-[2]

Further, secured availability of coal for around 200 years and as its cost being marginally increasing with time unlike other fossil fuels, it appears to be a suitable fuel material for meeting present and future energy demands. However, as observed by Mauna Loa Observatory, the recent atmospheric CO_2 level has touched an alarming level of 400ppm mark making it mandatory to develop clean, sustainable energy technologies for coal which can reduce CO_2 emission by capturing it in-situ. As chemical looping combustion is one such technology, a considerable amount of effort has been directed towards the development of this technology. Chemical looping process produces sequestration ready exhaust gases which mainly comprises of water and carbon dioxide from which water can be easily separated by the process of condensation.

Various simulation based investigations have been carried out on different segments of the above process such as a single reactor. One such CFD based study is by Deng *et al.* [3] on reaction kinetics of chemical looping combustion for fuel reactor only using FLUENT. They studied the effect of particle diameter, gas flow rate and bed temperature on fuel conversion. Further, a three dimensional CFD model for circulating fluidized bed fuel reactor has been developed by Wang *et al.* [4] using solid coal as a fuel and ilmenite ($FeTiO_3$) as an oxygen carrier. However, they have only evaluated the effect of operating variables on the fuel conversion of the fuel reactor. Furthermore, Wang *et al.* [5] developed a three dimensional numerical model for reactions between coal gas as fuel and cuprous oxide on alumina as an oxygen carrier for fuel reactor only considering kinetic theory of granular flow and analyzed the effects of the operating conditions such as bed height, bed temperature and operating pressure on fuel conversion. Though, Kruggel-Emden *et al.* [6] conducted an interconnected multiphase CFD simulation study of chemical looping combustion using methane as fuel and Mn_3O_4 supported on Mg-ZrO_2 as oxygen carrier for two separate systems, where bubbling fluidized bed is used for fuel reactor and riser as air reactor, their study did not include the interaction between the two reactors. In the absence of actual interaction study, they considered a time dependent mass exchange between these two reactors through inlet and outlet boundary conditions only.

Though, a considerable work has been carried out in the field of chemical looping, there appears to be substantive gap related to CFD based study of the complete process which incorporates the flow of material through fuel reactor, air reactor and their inter-connecting parts simultaneously to incorporate interaction between various parts of the process. To bridge the above gap, the present CFD simulation is carried out for a 25 kW_{th} complete pilot plant developed at Ohio State University, USA and discussed by Kim *et al.* [7]. They have discussed and reported the design criteria and operating conditions of the pilot plant wherein, two fuels namely sub-bituminous coal (SBC) and metallurgical coke (MC) have been used, one at a time, with iron (III) oxide supported on alumina as an oxygen carrier. They have considered eleven reactions that are taking place inside the fuel reactor and air reactor and their inter-connecting parts. A search in this regard, however shows that, they did not consider a few significant reactions for this purpose and neglected the effect of ash in the reactions. In the present work the CFD model is first verified against the reported results of the pilot plant data for the fuels SBC and MC. The model predicted values of fuel conversions for SBC and MC are 95.39% and 87.07% respectively

while; the literature reported values are 97% and 81%. Furthermore, the predicted purities of CO_2 in fuel reactor exhaust streams are 90.19% and 92.57% while; the reported values are 99.8% and 99.6% respectively for SBC and MC. After the validation of the present model, it is applied on two coals found in the region of Asia-Pacific and Australia having high ash content designated as A and B respectively.

2. Problem description:

In the chemical looping process, as proposed by Lewis and Gilliland [8], a carbonaceous fuel like natural gas, methane, coal, biomass, etc. first reacts in a fuel reactor with a metal oxide oxygen carrier such as iron oxide, nickel oxide, copper oxide, etc.. After reaction, this metal oxide gets reduced to metal and subsequently oxidizes the carbon present in the carbonaceous fuel. The above reaction yields carbon dioxide and steam as products from which carbon dioxide can readily be separated by removing steam through the process of condensation. The reduced metal received from the fuel reactor is oxidized in the air reactor for its regeneration to metal oxide, which is then recycled back to the fuel reactor for reuse. The above discussed cyclic process is shown in Fig. 1.

3. Problem Description:

Geometrical parameters of a 25 kW_{th} pilot plant developed by Ohio State University, USA and described in [7] have been considered for the present CFD simulation. The pilot plant geometry, taken from the thesis [9], is shown in Fig. 2 with dimension of different section in Table 1. Two different types of coal namely A and B having high ash contents are used one at a time in the pilot plant with iron (III) oxide as an oxygen carrier [7]. Both coal samples have been selected in such a way that these depict average composition in the range of compositions for coal and ash shown in Figs. 3 and 4. These figures cover overall variation in the components of coal found in the reserves of Asia-Pacific and Australia regions.

Tables 2 and 3 show the proximate analysis and ultimate analysis (on dry basis) for two coals i.e. A and B respectively that are used as fuels in the pilot plant described by [7]. Table 4 describes the composition of ash found in the coals used for simulation. Table 5 details properties of oxygen carrier that has been used for simulation.

Further, the ash has been classified into two types as reactive ash component and non-reactive ash component for simulation purpose; the reactive ash component includes SiO_2, Fe_2O_3, CaO while non-reactive ash components consist of the rest of ash components. Aluminum oxide being fairly inert is considered as a non-reactive component; while Magnesium oxide and Titanium dioxide are considered as non-reactive components as well because their presence (wt. %) in ash is very less (< 3 wt. %). On the other hand, Silica (SiO_2) being fairly inert (mass weighted rate of reaction in the order of 10^{-22}) is taken as a reactive component due to its reasonable presence in the ash composition.

4. Model Development:

A 2-D CFD model for the inter-connected fuel and air reactor is developed using commercial computational software Fluent 6.3.2 and mesh for above process layout has been developed using GAMBIT 2.3.16. The amount of gases injected in the system as well as generated from the reaction amounts to about 90% by volume. Thus, the gas and the mixture of solids are assumed to flow as a fluid inside both the reactors and their inter-connecting parts. This assumption has been used for the development of an approximate CFD model. Eleven reactions discussed in [7] along with 7 other significant reactions plus 6 reactions related to ash (not incorporated by [7]), as given in Table 6, 7 and 8, respectively are considered for the present CFD simulation. Before a complicated two phase CFD model is selected for the analysis for the present problem, it is thought logical to use the least complicated model, the Species-Transport model with volumetric reaction for the present study to check whether it validates the pilot plant data under acceptable error limits or not. Following governing equations are solved on commercially available software Fluent 6.3.2 for the present model:

Mass Conservation Equation:

The equation for mass conservation/continuity equation valid for compressible and incompressible flows can be written as:

$$\frac{\partial \rho}{\partial t} + \nabla . (\rho \vec{v}) = S_m \qquad ..(1)$$

Momentum Conservation Equations:

In an inertial frame, the momentum conservation equation is described as below Eq. 2:

$$\frac{\partial(\rho\vec{v})}{\partial t} + \nabla.(\rho\vec{v}\vec{v}) = -\nabla p + \nabla.(\bar{\bar{\tau}}) + \rho\vec{g} + \vec{F} \quad ..(2)$$

The stress tensor $\bar{\bar{\tau}}$ is given by Eq. 3

$$\bar{\bar{\tau}} = \mu\left[(\nabla\vec{v} + \nabla\vec{v}^T) - \frac{2}{3}\nabla.\vec{v}I\right] \quad ..(3)$$

The second term on the right hand side of Eq. 3 is the effect of volume dilation.

Energy Conservation Equation:

The conservation of Energy is defined by the following Eq. 4:

$$\frac{\partial(\rho E)}{\partial t} + \nabla.\left(\vec{v}(\rho E + p)\right) = \nabla.\left(k_{eff}\nabla T - \sum_j h_j\vec{J}_j + \left(\bar{\bar{\tau}}_{eff}.\vec{v}\right)\right) + S_h \quad ..(4)$$

$$E = h - \frac{p}{\rho} + \frac{v^2}{2} \quad ..(5)$$

Species Transport Equations:

The local mass fraction of each species (Y_i) through the solution of a convection-diffusion equation for the i^{th} species is solved. It takes the following general form:

$$\frac{\partial}{\partial t}(\rho Y_i) + \nabla.(\rho\vec{v}Y_i) = -\nabla.\vec{J_i} + R_i + S_i \quad ..(6)$$

Mass Diffusion in Laminar Flows:

In the above Eq. 6, this arises due to concentration gradients. In the present model, dilute approximation is assumed, under which it is defined as follows:

$$\vec{J_i} = -\rho D_{i,m}\nabla Y_i \quad ..(7)$$

The Laminar Finite-Rate Model:

The net source of chemical species i^{th} due to reaction is computed as the sum of the Arrhenius reaction sources over the N_R reactions that the species participate in:

$$R_i = M_{w,i} \sum_{r=1}^{N_R} \widehat{R_{i,r}} \quad ..(8)$$

Consider the r[th] reaction written in general form as follows in Eq. 9 which is valid for both reversible and non reversible reactions. For non-reversible reactions the backward rate constant is omitted.

$$\sum_{i=1}^{N} v'_{i,r} M_i \underset{k_{b,r}}{\overset{k_{f,r}}{\rightleftharpoons}} \sum_{i=1}^{N} v''_{i,r} M_i \quad ..(9)$$

For a non-reversible reaction, the molar rate of creation/destruction of specie i in reaction r ($\widehat{\mathbf{R}_{\mathbf{i,r}}}$in Eq. 8) is given by,

$$\widehat{R_{i,r}} = \Gamma\left(v''_{i,r} - v'_{i,r}\right)\left(k_{f,r} \prod_{j=1}^{N} [C_{j,r}]^{\left(\eta'_{j,r} + \eta''_{j,r}\right)}\right) \quad .. (10)$$

For a reversible reaction, the molar rate of creation/destruction of species i in reaction r, is given by,

$$\widehat{R_{i,r}} = \Gamma\left(v''_{i,r} - v'_{i,r}\right)\left(k_{f,r} \prod_{j=1}^{N} [C_{j,r}]^{\eta'_{j,r}} - k_{b,r} \prod_{j=1}^{N} [C_{j,r}]^{v''_{j,r}}\right) \quad ..(11)$$

The forward rate constant $k_{f,r}$ for reaction r, is computed using the Arrhenius expression

$$k_{f,r} = A_r T^{\beta_r} e^{-E_R/RT} \quad ..(12)$$

Values of $v'_{i,r}$, $v''_{i,r}$, $\eta'_{j,r}$,$\eta''_{j,r}$, β_r ,A_r and E_R are provided to solve Eq. 10

For reversible reactions, the backward rate constant $k_{b,r}$ for reaction r, is computed from the forward rate constant using the following relation:

$$k_{b,r} = \frac{k_{f,r}}{K_r} \quad ..(13)$$

The value of K_r is computed from the following Eq. 14

$$K_r = e^{\left(\frac{\Delta S_r^0}{R} - \frac{\Delta H_r^0}{RT}\right)} \left(\frac{p_{atm}}{RT}\right)^{\sum_{i=1}^{N}\left(v''_{i,r} - v'_{i,r}\right)} \quad ..(14)$$

Where, the term within the exponential function represents the change in Gibbs free energy, and its components are computed as follows:

$$\frac{\Delta S_r^0}{R} = \sum_{i=1}^{N}\left(v_{i,r}^{''} - v_{i,r}^{'}\right)\frac{S_i^0}{R} \quad ..(15)$$

$$\frac{\Delta H_r^0}{RT} = \sum_{i=1}^{N}\left(v_{i,r}^{''} - v_{i,r}^{'}\right)\frac{h_i^0}{RT} \quad ..(16)$$

Reactions Kinetics:

The present study is carried out for two types of coal A, and B; it utilizes 24 reactions for the process which are taking place inside two reactors and their inter-connecting parts. In Table 6, 11, reactions proposed by [7] are described while, in Tables 7 and 8, other seven significant reactions and reactions pertaining to reactive ash components with their kinetics are tabulated.

Standard k-ε turbulence model:

The standard k-ε turbulence model described by Launder and Spalding in 1974 is used for the present study.

Eq. 17 is described for turbulent kinetic energy k

$$\frac{\partial(\rho k)}{\partial t} + \frac{\partial(\rho k u_i)}{\partial x_i} = \frac{\partial}{\partial x_i}\left[(\mu + \frac{\mu_t}{\sigma_k})\frac{\partial k}{\partial x_j}\right] + G_k + G_b - \rho\epsilon - Y_M + S_k \quad ..(17)$$

And Eq. 18 is described for the rate of dissipation ε

$$\frac{\partial(\rho\varepsilon)}{\partial t} + \frac{\partial(\rho\varepsilon u_i)}{\partial x_i} = \frac{\partial}{\partial x_i}\left[(\mu + \frac{\mu_t}{\sigma_k})\frac{\partial \varepsilon}{\delta x_j}\right] + C_{1\varepsilon}\frac{\varepsilon}{k}(G_k + C_{3\varepsilon}G_b) - C_{2\varepsilon}\rho\frac{\varepsilon^2}{k} + S_\varepsilon \quad ..(18)$$

Where, G_k is calculated by Eq. 19, G_b is calculated by Eq. 20, Y_M is calculated by Eq. 21

$C_{1\varepsilon}$, $C_{2\varepsilon}$, $C_{3\varepsilon}$ are the constants ($C_{1\varepsilon}$ = 1.44, $C_{2\varepsilon}$ =1.92)

σ_k =1, σ_ε =1.3

$$G_k = -\rho\overline{u_i' u_j'}\frac{\partial u_j}{\partial x_i} \quad ..(19)$$

$$G_b = \beta g_i \frac{\mu_t}{Pr_t} \frac{\partial T}{\partial x_i} \quad ..(20)$$

Where, $Pr_t = 0.85$

$$Y_M = 2\rho\varepsilon M_t^2 \quad ..(21)$$

$M_t = \sqrt{\frac{k}{a^2}}$ and $a = \sqrt{\gamma RT}$

Mass-weighted average of rate of reaction:

The mass-weighted average of rate of reaction in different sections are computed by dividing, the summation of the values of the rate of reaction multiplied by the absolute value of the dot product of the facet area and momentum vectors, by the summation of the absolute value of the dot product of the facet area and momentum vectors as given in Eq.22:

$$\frac{\int \widehat{R_r}\, \rho|\vec{v}.d\vec{A}|}{\int \rho|\vec{v}.d\vec{A}|} = \frac{\sum_{i=1}^{n} \widehat{R_{i,r}} \rho_i |\overrightarrow{v_i}.\overrightarrow{A_i}|}{\sum_{i=1}^{n} \rho_i |\overrightarrow{v_i}.\overrightarrow{A_i}|} \quad ..(22)$$

5. Solution Technique:

In this section, solution technique adopted for the present study is described. The pilot plant dimensions are taken from the mechanical drawing of the pilot plant described in [7]. The boundary condition for air and coal inlets are defined as velocity inlet and mass flow inlet, while, fuel reactor and cyclone exhausts are defined as pressure outlets. Unsteady state simulations are carried out for present study and a time step of 0.001s is chosen for mesh grid size of 0.01(m) obtained from grid independence test for MC during model verification. The computational parameters used in present study are discussed in Table 9.

6. Result and Discussion:

In this section, the results obtained from the study of the effect of ash components present in coal during coal direct chemical looping combustion using the validated 2-D CFD model developed in present study is discussed. The previously developed model incorporating eighteen reactions for MC and SBC showed a better agreement with the pilot plant data. In present study only reaction kinetic aspect of ash is studied, the melting of ash and its associated effects, oxygen

carrier activity deactivation due to presence of ash, etc. are not incorporated. In the present CFD model, for both the fuels “A”, and “B”, six more reactions of reactive ash components are incorporated over and above eighteen reactions. While extending the present model to incorporate different types of ash bearing coals, the original dimensions of the pilot plant has not been specifically modified to suite the type of coal. Further, during the present simulation study, the limiting operating parameters like pressure drop, reactor bed temperature of the pilot plant have been kept within the limits fixed for the pilot plant.

In Fig. 5, a comparison between mass weighted averages rate of reactions (computed using Eq. 22) in four different sections of the process i.e. fuel reactor section, inter-connecting section, air reactor and riser section has been carried out. From Fig. 5 (a) & (c), it is clear that, coal devolatilization reaction (Reaction 1 [1.1, 1.2]) is the most dominating reaction in fuel reactor section, oxidation of iron to iron (III) oxide & combustion of left over carbon play a leading role in the air reactor. Further, water gas shift reaction is the most dominant in the inter-connecting pipe between fuel and air reactors as can be observed from Fig. 5 (b). In addition to above, in this section calcium hydroxide which is a product of reaction between CaO (present in reactive component of ash) with water forms plays a prominent role.

From Fig. 6 it can be seen that, whereas, fuel conversion for “A” and “B” are 93.8% and 87.89% respectively on coal basis, it is 89.12% and 90.73% for CO_2 purity in fuel reactor exhaust. Further, the normalized value of fuel flow rate, fuel reactor temperature and air reactor temperature for "A" and "B" fuel, when compared with the similar values of parameters for metallurgical coke, shows that the fuel reactor temperature remains slightly less than the metallurgical coke due to presence of high ash component and presence of reactive ash component which works as an oxygen carrier by transporting of oxygen from air reactor to fuel reactor. Moreover, the fuel requirement for feasible operation is about 1.5-2 times (for both A and B fuels) when compared to the amount of metallurgical coke that is required to sustain operation, and air reactor temperature increases due to combustion of left over carbon in that section.

In Table 10, the results of sensitivity analysis of the present CFD model are reported. The analysis is in respect to operating pressure of the system as well as air and fuel inlet temperatures on key output parameters such as CO_2 purity in fuel reactor exhaust, fuel conversion, and fuel

and air reactor temperature. It can be seen that the sensitivity of system for change in operating pressure is significant while, sensitivity for fuel and air inlet temperature is almost negligible.

7. Conclusion:

In present study, following salient features are observed:

1. Fuel conversion on dry ash free basis for fuel coals "A" and "B" are 93.8% and 90.73% respectively.

2. CaO and Fe_2O_3 as a part of reactive ash component shows reactivity under the process condition while SiO_2 exhibits a mass weighted average rate of reactions which is less than 10^{-20} kmol/m^3-s indicating that it works almost as an inert material.

3. The amount of ash present in fuel coal increases its fuel flow rate proportionately to maintain required feasible process conditions for chemical looping combustion. The carbon capturing efficiency decreases as fuel flow rate is increased. This observation is in conformity to Abad *et al.* [10]. Further, it can be seen that overall fuel conversion decreases as amount of non-carbonaceous species increases such as moisture and ash in the fuel coal as also been identified by Azis *et al.* [11]

4. The carbon dioxide purity in fuel reactor exhaust increases with the rise in fuel reactor temperature for the two fuels used in the present study. This fact is in tune with the observations of Abad *et al.* [10] carried out for El Cerrejón coal with less than 10% ash content.

8. Nomenclature

A_r	pre-exponential factor
β	coefficient of thermal expansion
β_r	temperature exponent

$C_{j,r}$	molar concentration of species j in reaction r
$D_{i,m}$	diffusion coefficient for the i^{th} species in the mixture
ε	the rate of dissipation
E_R	activation energy for the reaction
$\vec{F}$	external body forces and also contains user-defined terms
$\gamma_{j,r}$	third-body efficiency of the j^{th} species in the r^{th} reaction
g_i	gravitational vector in the i^{th} direction
G_b	the generation of turbulence kinetic energy due to buoyancy
G_k	generation of turbulence kinetic energy due to mean velocity gradients
h^0_i	standard-state enthalpy (heat of formation) which are specified as properties for every species
I	unit tensor
$\vec{J_i}$	diffusion flux of the i^{th} species,
$\vec{J_j}$	diffusion flux of species j
K	turbulent kinetic energy
$k_{b,r}$	backward rate constant for reaction r
k_{eff}	effective conductive ($=k+k_t$)
$k_{f,r}$	forward rate constant for reaction r
k_t	turbulent thermal conductivity
K_r	equilibrium constant for the r^{th} reaction
M	molecular viscosity
μ_t	turbulent viscosity
M_i	symbol denoting species i
M_t	turbulent Mach number
$M_{w,i}$	molecular weight of i^{th} species
$\eta'_{j,r}$	rate exponent for reactant species j in reaction r
$\eta''_{j,r}$	rate exponent for product species j in reaction r

N	number of chemical species in the system
P	static pressure
p_{atm}	atmospheric pressure (101.325 kPa)
Pr_t	turbulent Prandtl number for energy
$\rho\vec{g}$	gravitational body force
R	universal gas constant
R_i	net rate of production of species i by chemical reaction
$\widehat{\mathbf{R_{i,r}}}$	Arrhenius molar rate of creation/destruction of species i^{th} in reaction r
σ_ε	turbulent Prandtl number for ε
σ_k	turbulent Prandtl number for k
S_ε	User defined source term
S_h	the heat of chemical reaction and any other volumetric source by user defined function
S_i	rate of creation by addition from dispersed phase plus any user defined sources
S^0_i	standard-state entropy which are specified as properties for every species
S_k	User defined source term
S_m	mass added to continuous phase from second phase or any user-defined sources
$\bar{\bar{\tau}}$	stress tensor
Γ	the net effect of third bodies on the reaction rate
$\nu'_{i,r}$	stoichiometric coefficient for reactant i in reaction r
$\nu''_{i,r}$	stoichiometric coefficient for product i in reaction r
Y_j	the mass fraction of species j
Y_M	the contribution of the fluctuating dilation in compressible turbulence to the overall dissipation rate

9. References:

[1] BP Statistical Review of World Energy, June 2013

[2] Energy Information Administration, "International Energy Outlook 2006", U.S. Department of Energy, Washington DC, 2006

[3] Zhongyi Deng, Rui Xiao, Baosheng Jin, Qilei Song, He Huang, "Multiphase CFD Modeling for a Chemical Looping Combustion Process (Fuel Reactor)", Chemical Engineering Technology, Vol. 31, Issue 12, 2008, pp.1754-1766

[4] Xiaojia Wang, Baosheng Jin, Yong Zhang, Yi Zhang, Xianli Liu, "Three Dimensional Modeling of a Coal-Fired Chemical Looping Combustion Process in the Circulating Fluidized Bed Fuel Reactor", Energy & Fuels, Vol. 27, 2013, pp. 2173-2184

[5] Xiaojia Wang, Baosheng Jin, Yong Zhang, Wenqi Zhong, Shangyi Yin, "Multiphase Computational Fluid Dynamics (CFD) modeling of chemical looping combustion using a CuO/Al_2O_3 oxygen carrier: effect of operating conditions on coal gas combustion", Energy & Fuels, Vol. 25, 2011, pp. 3815-3824

[6] H. Kruggel-Emden, S.Rickelt, F.Stepanek, A.Munjiza, "Development and testing of an interconnected multiphase CFD-model for chemical looping combustion", Chemical Engineering Sciences, Vol. 65, 2010, pp. 4732-4745

[7] Hyung R. Kim, Dawei Wang, Liang Zeng, Samuel Bayham, Andrew Tong, Elena Chung, Mandar V. Kathe, Siwei Luo, Omar McGiveron, Aining Wang, Zhenchao Sun, David Chen, Liang-Shih Fan, "Coal direct chemical looping combustion process: Design and operation of a 25-kW_{th} sub-pilot unit", Fuel, Vol. 108, 2013, pp. 370-384

[8] L.S. Fan, Chemical looping systems for fossil energy conversion, A John Wiley & sons Inc., publication, 2010

[9] Rahul Wadhwani, "CFD study of a coal direct chemical looping pilot plant", IDD Thesis, Indian Institute of Technology Roorkee, Roorkee, India, 2014

[10] A. Abad, J. Adánez, L. F. de Deigo, P. Gayán, F. G. Labiano, A. Lyngfelt, "Fuel reactor model validation: Assessment of the key parameters affecting the chemical looping combustion of coal", International Journal of Greenhouse Gas Control, Vol. 19, 2013, pp. 541- 551

[11] M. M. Azis, H. Leion, E. Jerndal, B. M. Steenari, T. Mattison, A. Lyngfelt, “The effect of bituminous and lignite ash on the performance of ilmenite as oxygen carrier in chemical looping combustion”, Chemical Engineering Technology, Vol. 36, 2013, pp. 1460-1468

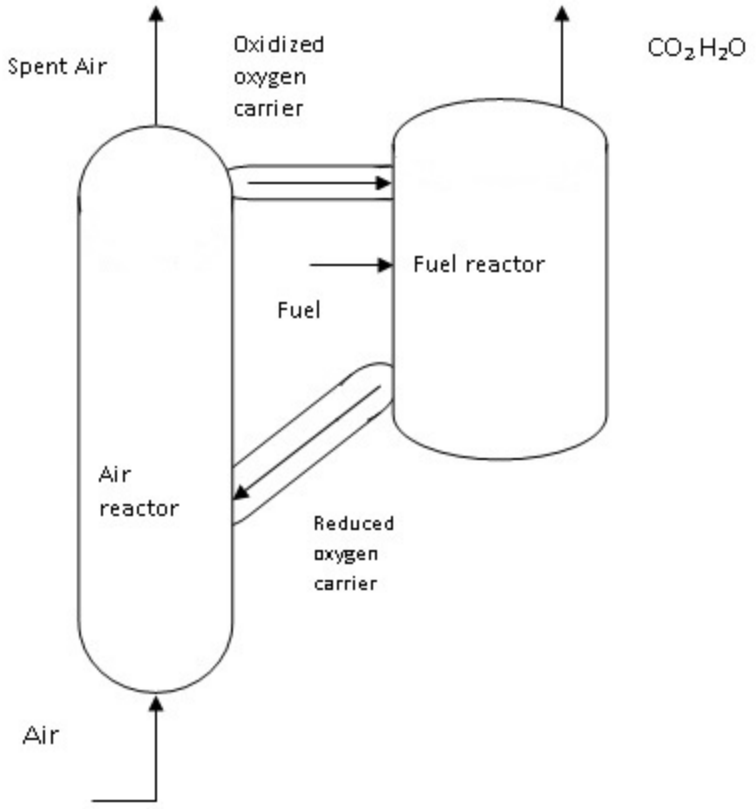

Fig. 1: Process overview

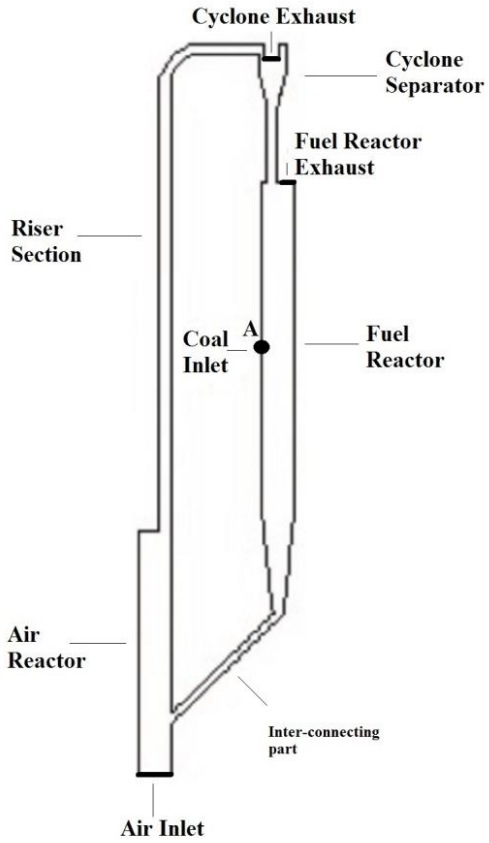

Fig. 2: Pilot plant of present problem

Table 1: Geometry Parameters

Fuel Reactor Height	3.37m
Fuel Reactor Diameter	0.34m
Air Reactor Height	1.88m
Air Reactor Diameter	0.33m
Tube Diameter	0.11m
Riser Height	4.68m
Cyclone Separator Total Height	0.62m
Cyclone Separator Diameter	0.28m

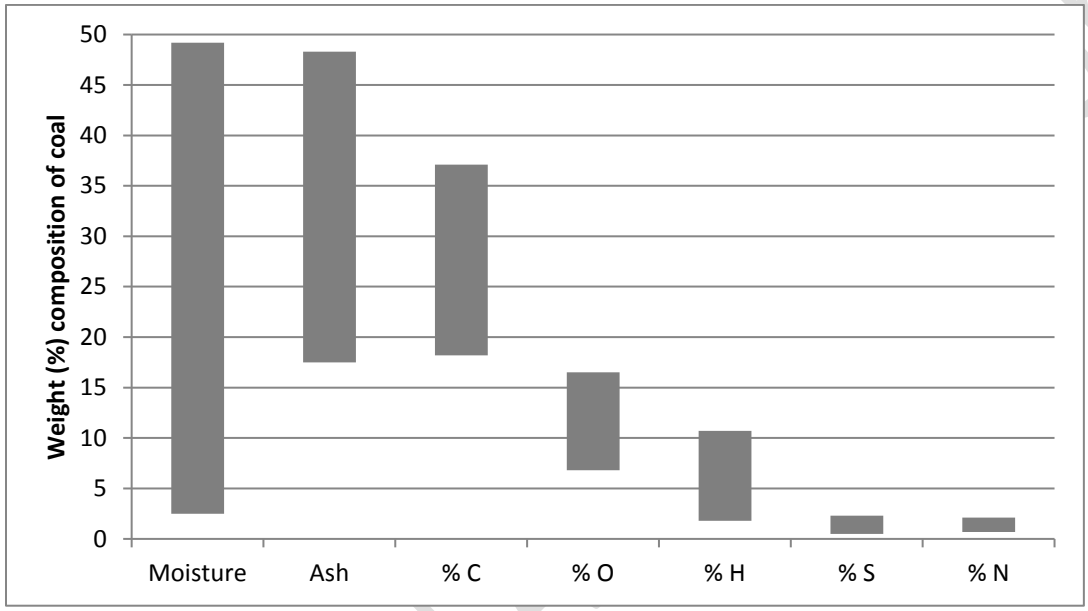

Fig. 3: Variation in coal compositions found in regions of Asia-Pacific and Australia

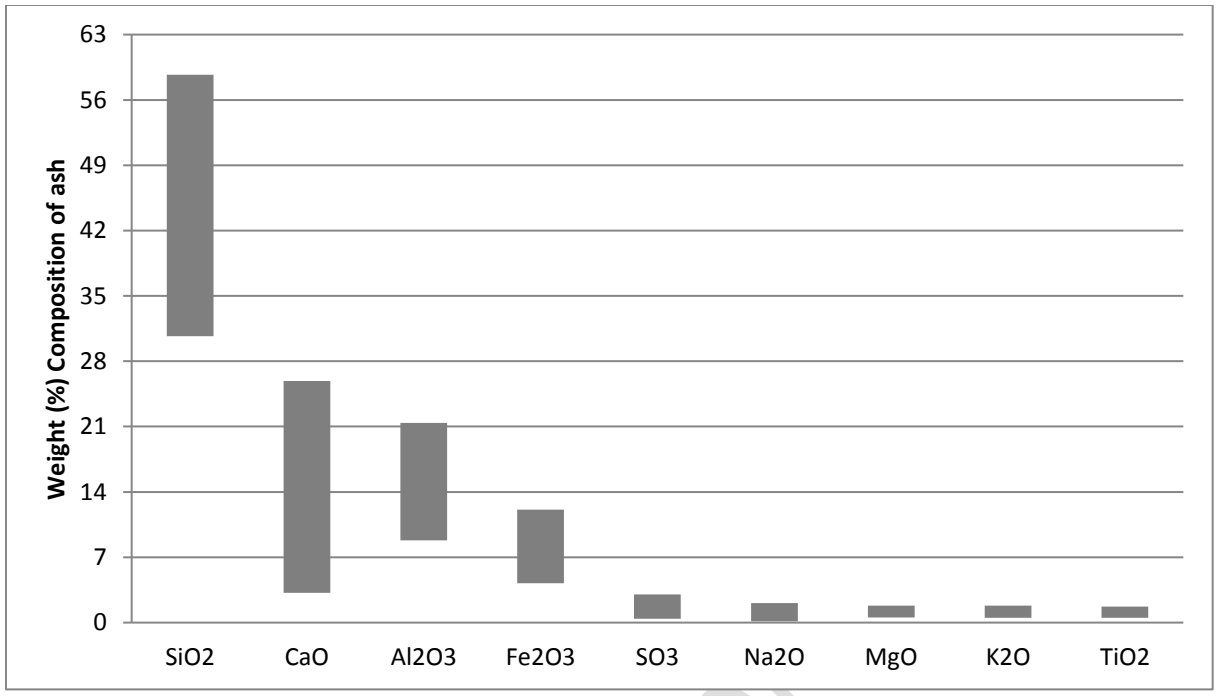

Fig.4: Variation in Ash composition of coals found in regions of Asia-Pacific and Australia

Table 2: Proximate Analysis of fuels

	Proximate Analysis (Dry Basis)	
	A	B
Ash	25.87%	31.5%
Volatile Matter	29.87%	7.5%
Fixed Carbon	42.86%	59.9%
Energy Value	26,120	23,398
Energy Value[1]	30,729	27,527
Average Particle Size	125 μm	100 μm
Moisture	1.4%	1%

[1] moisture and ash free

Table 3: Ultimate Analysis of fuels

	Ultimate Analysis (Dry Basis)	
	A	B
Carbon	61.76%	56.7%
Hydrogen	4.16%	3.2%
Nitrogen	0.76%	0.9%
Sulfur	0.91%	0.6%
Oxygen	5.14%	6.1%

Table 4: Ash compositions of Fuels

Components	Fuels Composition	
	A	B
SiO_2	54.18%	48.34%
Al_2O_3	32.84%	28.12%
Fe_2O_3	5.35%	11.88%
TiO_2	2.27%	1.6%
CaO	1.57%	7.17%
SO_3	1.47%	0.68%
MgO	0.53%	1.13%
Na_2O	0.41%	0.6%
K_2O	1.39%	0.48%

Table 5: Properties of oxygen carrier

Reactive oxygen carrier	Fe_2O_3
Weight content of reactive oxygen carrier	40-60%
Average particle size of oxygen carrier	1.5 mm
Supporting oxygen carrier	Al_2O_3
Density of oxygen carrier	4724 kg/m^3

Table 6: Reactions proposed by [7] for coal direct chemical looping process

Reaction No.	Reaction	E_R (J/kmol)
1.	$Coal \rightarrow C + CH_4 + NO_2 + SO_2 + CO_2 + H_2O$	
1.1	**For A:** $C_{7.07}H_{5.67}N_{0.07}S_{0.04}O_{0.44} \rightarrow 5.6425C + 0.06CO_2 + 0.07NO_2 + 0.04SO_2 + 0.1H_2O + 1.3675CH_4$	8.5×10^7
1.2	**For B:** $C_{6.99}H_{4.71}N_{0.095}S_{0.027}O_{0.565} \rightarrow 5.773C + 0.121H_2O + 0.095NO_2 + 0.027SO_2 + 1.117CH_4 + 0.1CO_2$	9.7×10^7
2.	$2Fe_2O_3 + C \rightarrow 4\,FeO + CO_2$	3.0124×10^8
3.	$4Fe_2O_3 + CH_4 \rightarrow 8FeO + 2H_2O + CO_2$	1.352×10^8
4.	$Fe_2O_3 + CO \rightarrow 2FeO + CO_2$	8.07×10^7
5.	$Fe_2O_3 + H_2 \rightarrow 2FeO + H_2O$	6.5×10^7
6.	$FeO + CO \rightarrow Fe + CO_2$	1.205×10^7
7.	$FeO + H_2 \rightarrow Fe + H_2O$	2.151×10^7
8.	$C + CO_2 \rightarrow 2CO$	2.11×10^8
9.	$C + H_2O \rightarrow CO + H_2$	2.31×10^8
10.	$2Fe + 1.5O_2 \rightarrow Fe_2O_3$	2.025×10^7
11.	$2FeO + 0.5\,O_2 \rightarrow Fe_2O_3$	2.55×10^7

Table 7: Other significant reactions for coal direct chemical looping process

Reaction No.	Reaction	E_R (J/kmol)
12.	$C + 2H_2 \rightarrow CH_4$	1.5×10^8
13.	$CO + H_2O \rightleftharpoons CO_2 + H_2$	1.26×10^7
14.	$CH_4 + H_2O \rightleftharpoons CO + 3H_2$	3×10^7
15.	$C + O_2 \rightarrow CO_2$	1.794×10^8
16.	$CO + 0.5\, O_2 \rightarrow CO_2$	1.674×10^8
17.	$2FeO + H_2O \rightarrow Fe_2O_3 + H_2$	7.79×10^7
18.	$2H_2 + O_2 \rightarrow 2H_2O$	2.852×10^7

Table 8: Reaction kinetics of reactive ash component

Reaction no.	Reaction	E_R (J/kmol)
19.	$CaO + CO_2 \rightarrow CaCO_3$	1.59×10^8
20.	$CaO + H_2O \rightarrow Ca(OH)_2$	1.744×10^7
21.	$Ca(OH)_2 + CO_2 \rightarrow CaCO_3 + H_2O$	9.92×10^6
22.	$SiO_2 + C \rightleftharpoons SiO + CO$	3.28×10^8
23.	$SiO + 2C \rightleftharpoons SiC + CO$	3.82×10^8
24.	$SiO + 3CO \rightleftharpoons SiC + CO_2$	2.741×10^8

Table 9: Computational and Simulation Parameters for the Present Study

Operating Pressure	10 atm		
Air Inlet Velocity	0.001 m/s		
Fuel Flow rate for A	2 kg/h		
Fuel Flow rate for B	2.25 kg/h		
Air and Fuel inlet Temperature	320 K		
Carrier CO_2 gas flow rate	10 LPM		
Under Relaxation Factors			
Pressure	0.1	Density	0.1
Momentum	0.1	Body Forces	0.1
Turbulent Kinetic Energy	0.1	Species	0.1
Turbulent Dissipation Rate	0.1	Energy	0.1
Model Parameters			
Solver	Unsteady State, 2^{nd} order implicit		
Discretization Scheme	Second order Upwind		
Pressure Velocity Coupling	SIMPLE		
Time step	0.001s		
Iteration per time step	30		
Convergence Criterion	10^{-5}		

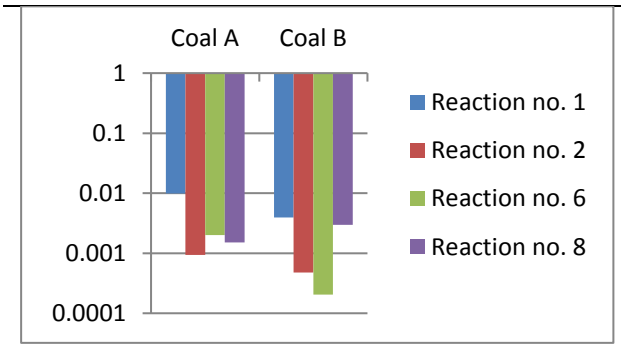

(a) Fuel Reactor section

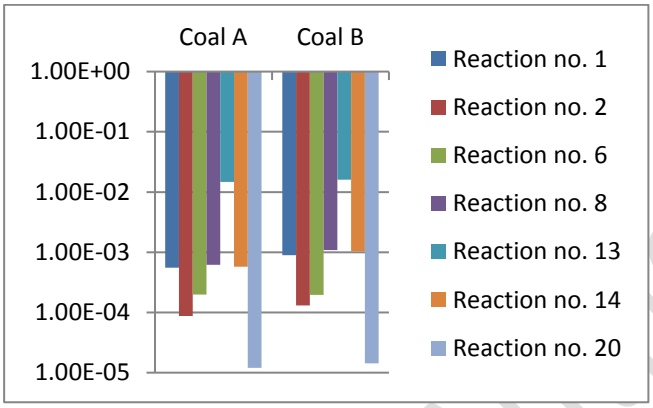

(b) Inter-connecting section

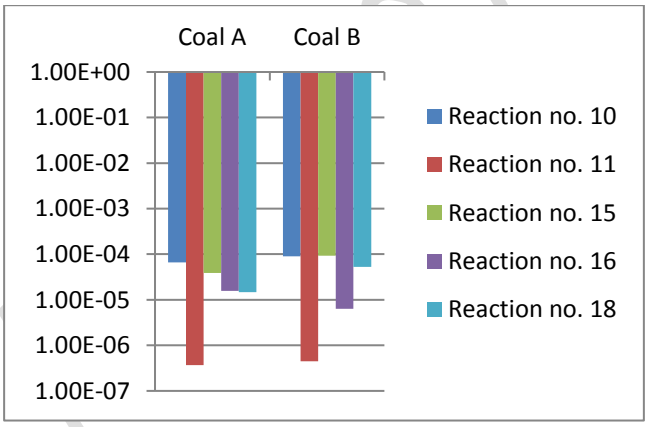

(c) Air reactor section

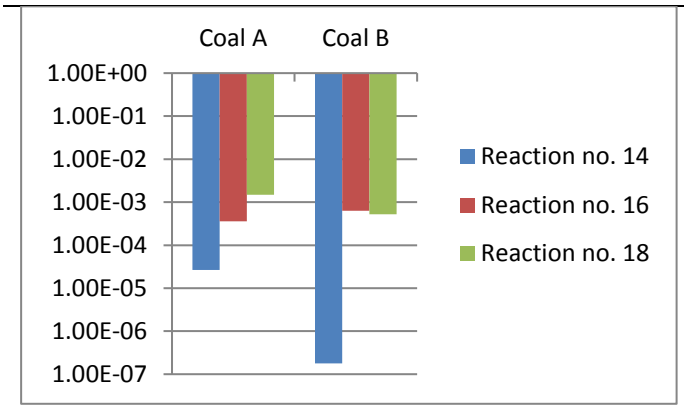

(d) Riser section

Fig. 5: Mass weighted average rate of most dominating reactions in four sections of the process

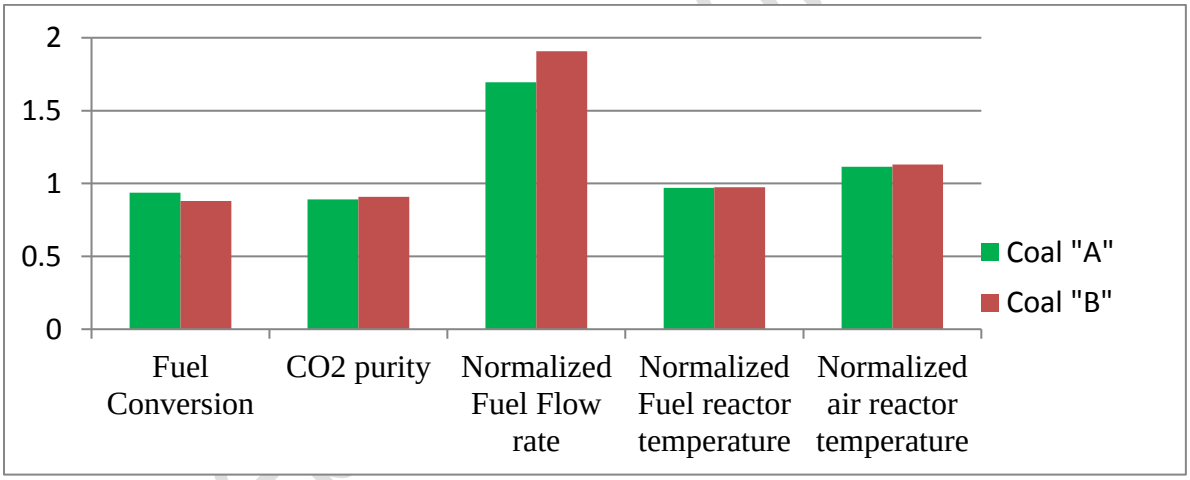

Fig. 6: Comparative results for coal “A” and “B”

Table 10: Sensitivity analysis of operating pressure and fuel & air inlet temperature

Variable	CO_2 purity	Fuel conversion	Fuel reactor temperature (K)	Air reactor temperature (K)
Operating Pressure	Coal A			
10 atm	89.12%	93.8%	1208	1076
15 atm	89.46%	93.5%	1200	1072
	Coal B			
10 atm	90.73%	87.89%	1214	1090
15 atm	90.46%	87.53%	1209	1083
Fuel and Air Inlet temperature	Coal A			
320 K	89.12%	93.8%	1208	1076
330 K	89.11%	93.81%	1209	1077
	Coal B			
320 K	90.73%	87.89%	1214	1090
330 K	90.72%	87.91%	1214	1092